Transient, Stratified, Enclosed Gas and Liquid Behavior with Concentrated Heating from Above

B. Abramzon,* D. K. Edwards,† and W. A. Sirignano‡
University of California, Irvine, California

A computational study has been made of transient heat transfer and fluid flow in a cylindrical enclosure containing a two-layer gas-and-liquid system. The geometric configuration and the boundary conditions on the problem are relevant to the analysis of the prevaporization and preignition processes during the fire accident situation involving a pool of liquid fuel in the vicinity of an ignition source. It is demonstrated that the effects of the natural and thermocapillary convection, radiative transfer, and thermal inertia and conduction of the walls bounding the enclosure and the magnitude of the gravity field play important roles in the development of the temperature and velocity fields in the container.

Introduction

WHEN a concentrated source of heat is placed above a pool of liquid fuel, a number of complex thermophysical processes are induced preceding the ignition of the fuel vapors. If the initial liquid fuel temperature is below the flash point, a substantial amount of thermal energy may be required to evaporate some portion of the fuel and to create a combustible vapor air mixture. This energy is supplied from the hot source by several heat-transfer mechanisms, including heat conduction through the gas phase, natural convection induced in the gas near the source, and thermal radiation. The heat flux to the liquid surface is largest directly under the source and decreases monotonically with the distance from the hot source. The nonuniform heating of the fuel induces both buoyancy and surface-tension-driven currents in the subsurface liquid layer. The latter effect is caused by the gradient in surface tension due to the temperature variation along the gas liquid interface.

The first stage of the preignition period essentially consists of heating the liquid fuel near the surface. The second stage starts when the partial pressure of the fuel vapor becomes sufficient to yield a combustible mixture with the air above the fuel. At this stage (and during flame spreading), evaporation, diffusion, and chemical reactions play an important role.

An experimental study of liquid pool ignition has been reported by Murad et al.[1] In particular, it was found that the heating of a fuel to the point of ignition is retarded considerably by the surface-tension-driven currents induced in the pool. Sirignano and Glassman[2] found that the same subsurface flows also govern the process of the flame spreading over liquid fuels. The latter phenomenon has been extensively studied by many authors. A comprehensive review on the subject is presented in the recent paper by Furita et al.[3] These authors performed also a finite-difference study of a steady laminar flame spread over the shallow fuel pool. Momentum, energy, and mass conservation equations were solved simultaneously both in the gas and liquid phases. The combustion process was modeled using the flame sheet approximation. Radiative transport was neglected.

In contrast to steady-state flame spread, transient ignition has not been treated theoretically in the literature. However, such a problem is relevant to many fire hazard situations. For example, the prototypical accident situation might be the case when an external fire source results in a sudden temperature increase on one part of the fuel tank wall.

In the present paper, we consider the initial (prevaporization and preignition) stage for the geometry shown in Fig. 1. Here, the cylindrical enclosure of radius R' and height $H' = H'_g + H'_\ell$ contains a two-layer gas/liquid system. The initial temperature of the system is uniform at $T' = T'_0$. At time zero ($t' = 0$), the temperature of a small circular spot of radius R' at the center of the top cover increases suddenly to $T' = T'_h \gg T'_0$ and then remains constant. The fluids can be subject to a reduced gravity such as exists in space flight vehicles. As is known, gravity is an important parameter in both buoyancy and thermocapillary phenomena (see Ref. 15).

Note that an analysis of transient heat transfer and hydrodynamics for a similar geometry was conducted by Aggarwal et al.[4] The present study examines the influence of some important factors, such as thermal radiation and the thermal inertia and conductance of the container's walls.

Statement of the Problem

The mathematical formulation of the problem is based on the following general assumptions:

1) Both the gas and liquid kinematic viscosities (ν_g, ν_ℓ), thermal diffusivities (α_g, α_ℓ), and volume thermal expansion coefficients (β_g, β_ℓ) are constant. Both fluids are taken to have constant densities (ρ_g, ρ_ℓ), except in the buoyancy force terms (Boussinesq approximation).

2) The problem is axisymmetric and the gas/liquid interface remains flat and horizontal. The latter assumption is valid if the Bond number, $Bo = (\rho_\ell - \rho_g) g R'^2/\sigma$, estimating the relative importance of the gravitational and surface tension forces, is sufficiently large: $Bo \gg 1$.

3) All of the solid surfaces as well as the gas/liquid interface are assumed opaque and black and gas radiation is neglected.

4) The walls bounding the enclosure are taken to be so thin that the temperature drop across the thickness is negligible (the "fin" approximation). The top and side walls are adiabatically isolated from the environment; however, the wall temperature may change spatially and with time as a result of the convective heat exchange with the fluids, the radiative transfer between the different surfaces, and the thermal conduction along the walls. The hot spot has no thermal contact with the remaining part of the top cover. The bottom wall is maintained at the constant temperature $T' = T'_0$.

5) Liquid vaporization, diffusion, chemical reactions, and radiative absorption in the gas phase are neglected.

Received July 21, 1986; revision received Nov. 3, 1986.

*Research Associate, Department of Mechanical Engineering.
†Professor of Mechanical Engineering, Associate Dean of Engineering.
‡Professor of Mechanical Engineering, Dean of Engineering.

With primes denoting dimensional quantities, the following characteristic values and nondimensional variables are introduced:

Reference time, $t'_* = R'^2/\nu_g$

Reference velocity, $U'_* = R'/t'_*$

Reference pressure, $\Delta P'_* = \rho_g U'^2_*$

Reference temperature difference, $\Delta T'_* = T'_h - T'_0$

Radial and axial coordinates, $r = r'/R'$ and $y = y'/R'$

Radial and axial velocity components $u = u'/U'_*$ and $v = v'/U'_*$

Pressure, $P = P'/\Delta P'_*$

Temperature, $T = (T' - T'_0)/\Delta T'_*$

Note that the reference values of t'_*, U'_*, and $\Delta P'_*$ are defined using the physical properties of the gas.

The conservation equations of mass, momentum, and energy in each phase are written in nondimensional form as follows:

Continuity equation

$$\frac{\partial u}{\partial r} + \frac{\partial v}{\partial y} + \frac{u}{r} = 0 \tag{1}$$

Momentum equation in radial direction

$$\frac{\partial u}{\partial t} + \frac{\partial u^2}{\partial r} + \frac{\partial uv}{\partial y} + \frac{u^2}{r} = -Eu_i \frac{\partial P}{\partial r} + \frac{1}{Re_i}\left(\frac{\partial^2 u}{\partial r^2} + \frac{\partial^2 u}{\partial y^2} + \frac{1}{r}\frac{\partial u}{\partial r} - \frac{u}{r^2}\right) \tag{2}$$

Momentum equation in axial direction

$$\frac{\partial v}{\partial t} + \frac{\partial uv}{\partial r} + \frac{\partial v^2}{\partial y} + \frac{uv}{r} = -Eu_i \frac{\partial P}{\partial y} + Gr_i \frac{1}{Re_i^2} T + \frac{1}{Re_i}\left(\frac{\partial^2 v}{\partial r^2} + \frac{\partial^2 v}{\partial y^2} + \frac{1}{r}\frac{\partial v}{\partial r}\right) \tag{3}$$

Energy equation

$$\frac{\partial T}{\partial t} + \frac{\partial (uT)}{\partial r} + \frac{\partial (vT)}{\partial y} + \frac{uT}{r} = \frac{1}{Re_i Pr_i}\left(\frac{\partial^2 T}{\partial r^2} + \frac{1}{r}\frac{\partial T}{\partial r} + \frac{\partial^2 T}{\partial y^2}\right) \tag{4}$$

where the subscript $i = g$ or ℓ refers to the gas or liquid phase, respectively.

The dimensionless Reynolds, Euler, Prandtl, and Grashof numbers are defined or each phase as follows:

$$Re_i = U'_* R'/\nu_i \qquad Eu_i = \Delta P'_*/(\rho_i U'^2_*)$$

$$Pr_i = \nu_i/\alpha_i \qquad Gr_i = g\beta_i R'^3 \Delta T'_*/\nu_i^2$$

Note that in the present formulation, the Reynolds and Euler numbers are constant: $Re_g = Eu_g = 1$, $Re_\ell = \nu_g/\nu_\ell$, and $Eu_\ell = \rho_g/\rho_\ell$.

The hydrodynamic boundary conditions are as follows:

1) Zero velocity on all solid walls,

$$u = v = 0 \tag{5}$$

2) Symmetry of the velocity field at the axis $r = 0$,

$$u = 0, \quad \frac{\partial v}{\partial r} = 0 \tag{6}$$

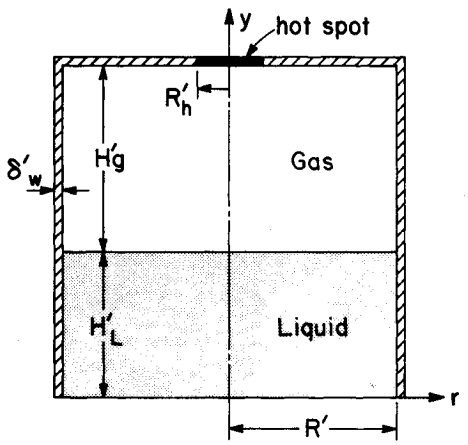

Fig. 1 Geometry of the problem.

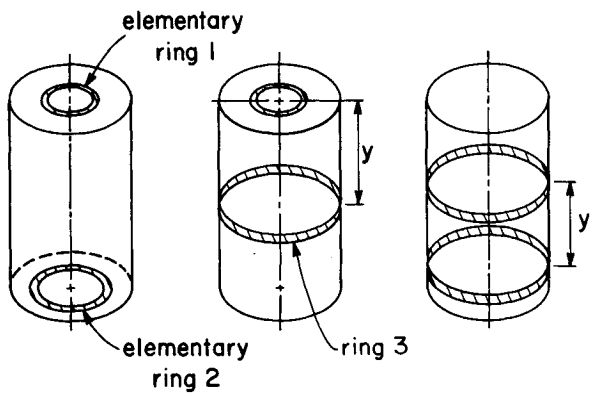

Fig. 2 Radiative heat transfer between different elementary rings on the walls and the liquid surface.

3) Balance of the stresses and continuity of the velocity components on the gas/liquid interface,

$$\left(\frac{\partial u}{\partial y}\right)_\ell = \frac{\Delta T'_*}{U'_* \mu_\ell}\left(\frac{\partial \sigma}{\partial T'}\right)\left(\frac{dT}{dr}\right)_{\ell g} + \frac{\mu_g}{\mu_\ell}\left(\frac{\partial u}{\partial y}\right)_g \tag{7}$$

$$v_g = v_\ell = 0, \quad u_g = u_\ell \tag{8}$$

where $\mu = \rho\nu$ is the dynamic viscosity and $\sigma = \sigma(T')$ the surface tension.

The thermal boundary conditions are as follows:

1) Constant temperature of the "hot spot" ($r < r_h, y = H'/R$),

$$T = 1 \tag{9}$$

2) Constant temperature at the bottom end of the tank ($y = 0$),

$$T = 0 \tag{10}$$

3) Heat balance and continuity of the temperature on the gas/liquid interface,

$$k_\ell \left(\frac{\partial T}{\partial y}\right)_\ell - k_g \left(\frac{\partial T}{\partial y}\right)_g = \frac{q'_R R'}{\Delta T'_*} \tag{11}$$

$$T_g = T_\ell \tag{12}$$

4) Transient heat conduction equations governing the one-dimensional temperature distribution in the side and top walls,

$$\frac{\partial T_w}{\partial t}=\frac{q'}{q'_{w,*}}+\frac{\alpha_w}{\nu_g}\left(\frac{\partial^2 T_w}{\partial y^2}\right) \tag{13}$$

at $r=1$ and $0<y<H'/R'$, and

$$\frac{\partial T_w}{\partial t}=\frac{q'}{q'_{w,*}}+\frac{\alpha_w}{\nu_g}\left(\frac{\partial^2 T_w}{\partial r^2}+\frac{1}{r}\frac{\partial T_w}{\partial r}\right) \tag{14}$$

at $y=H'/R'$ and $r_h<r<1$.

In the above equations, T_w is the local wall temperature; $q'=q'_R+q'_c$ the local dimensional heat flux including the radiative and convective components; $q'_{w,*}=\rho_w C_w \delta_w \Delta T'_*/t'_*$ the characteristic value of heat flux that must be supplied to an isolated wall to increase its temperature to $\Delta T'_*$ during time t'_*; δ_w the thickness of the wall; and ρ_w, C_w, and α_w the density, heat capacity, and thermal diffusivity of the wall, respectively.

The convective component of the local heat flux to the wall q'_c is expressed as:

$$q'_c=-\left(\frac{k_i \Delta T'_*}{R'}\right)\left(\frac{\partial T_i}{\partial n}\right)_w$$

where $i=g;\ell$ and $(\partial T_i/\partial n)_w$ is the nondimensional normal derivative of the temperature near the wall.

Method of Solution

Calculation of the Radiation Fluxes

Consider differential ring elements on the internal surfaces (see Fig. 2): ring 1 of radii $r'_1 \pm \Delta r'_1/2$ on the top cover, ring 2 of radii $r'_2 \pm \Delta r'_2/2$ on the liquid surface, and ring 3 of radius R' and height $\Delta y'$ on the interior of the cylinder. The heat transferred by radiation between two elementary rings j,k is calculated as

$$\Delta Q'_{jk}=\sigma_B (T'^4_j - T'^4_k)\Delta A'_j \Delta A'_k \phi_{jk} \tag{15}$$

where $\Delta A'_j$ is the area of the jth ring, T'_j the mean absolute temperature of the ring, σ_B the Stefan-Boltzmann constant, and ϕ_{jk} the shape factor kernel related to the configuration factors F_{jk} or F_{kj} by[5]

$$\phi_{jk}=F_{jk}/\Delta A'_k=F_{kj}/\Delta A'_j$$

The expressions for ϕ_{jk} are

$$\phi_{12}=\phi_{21}=\frac{H_g^2[H_g^2+r_1^2+r_2^2]}{\pi R'^2[(H_g{}^2+r_1^2+r_2^2)^2-4r_1^2r_2^2]^{3/2}} \tag{16}$$

$$\phi_{13}=\phi_{31}=\frac{y(1+y^2-r_1^2)}{\pi R'^2[(1+y^2+r_1^2)^2-4r_1^2]^{3/2}} \tag{17}$$

$$\phi_{33}=\frac{1}{4\pi R'^2}\left[1-\frac{(y^3+6y)}{(y^2+4)^{3/2}}\right] \tag{18}$$

where $H_g=H'_g/R'$, $r=r'/R'$, $y=y'/R'$, and y' is the distance between the planes of two ring elements (Fig. 2). The values of $\phi_{23}=\phi_{32}$ are calculated similar to ϕ_{13} (except that r_1 is replaced by r_2). To find the local radiation flux q'_R, Eq. (15) was integrated numerically over all radiant surfaces.

Numerical Method

The finite-difference procedure applied to the hydrodynamic equations is a modification of the SMAC method developed at Los Alamos Laboratory.[6,7] This method utilizes the primitive variables (u,v,p) and a staggered mesh.[7,11] The fluid velocities $u_{i,j}$ and $v_{i,j}$ are located at the middle of the right and top sides of the (i,j) cell, respectively. The pressure and temperature are calculated at the center of the cell. The fluid domain is surrounded by a single layer of ficticious cells that are used to set the boundary conditions.

To demonstrate the principal idea of the numerical approach, we will use the vector form of the Navier-Stokes equations,

$$\frac{\partial v}{\partial t}+(v\nabla)v=-\frac{Gr}{Re^2}\left(\frac{g}{g}\right)T-Eu\nabla P+\frac{1}{Re}\nabla^2 v \tag{19}$$

$$\operatorname{div} v=0 \tag{20}$$

Assume that the velocity and pressure fields are known at time t: $v=v_t$ and $P=P_t$. To calculate the acceleration $\partial v/\partial t$ in Eq. (19), the pressure gradient is approximated in the implicit form (at the time level $t+\Delta t$), while all terms containing velocities are written using the previous state of the flow. Then, the finite-difference approximation of momentum equation (19) is expressed as

$$v_{t+\Delta t}=\tilde{v}_{t+\Delta t}-Eu\Delta t\nabla(\delta P) \tag{21}$$

where $\delta P=P_{t+\Delta t}-P_t$ is the pressure change during the time step Δt and

$$\tilde{v}_{t+\Delta t}=v_t+\Delta t\left\{-\frac{Gr}{Re^2}\left(\frac{g}{g}\right)T-(v\nabla)v-Eu\nabla P+\frac{1}{Re}\nabla^2 v\right\}_t \tag{22}$$

is the "tilde" velocity field representing a first, explicit guess of the velocity field at the next time level.

The new velocity field $v_{t+\Delta t}$ must satisfy continuity equation (20). Taking the divergence of Eq. (21) gives

$$\nabla^2(\delta P)=\frac{1}{Eu\Delta t}\operatorname{div}(\tilde{v}_{t+\Delta t}) \tag{23}$$

This is the Poisson equation for the pressure correction δP. The boundary conditions for Eq. (23) are

$$\frac{\partial(\delta P)}{\partial n}=0 \tag{24}$$

In the original SMAC method,[6] the Poisson equation is solved using the SOR technique. In the present study, the faster ADI method with cyclical selection of the iteration parameter[8] was applied. Using the ADI method with Wachspress iteration parameters gave a considerable saving (by a factor of 3:4) of the computation time in comparison with the original SOLA program.[7]

Equation (23) is written in the "pseudo unsteady" form as

$$\frac{\partial Z}{\partial \tau}=\nabla^2 Z-\tilde{D}_{t+\Delta t} \tag{25}$$

where $Z=Eu\Delta t\delta P$, $D=\operatorname{div} v$, and the false-transient term $\partial(Z)/\partial\tau$ is introduced in order to apply the ADI method. The "time step" $\Delta\tau$ plays the role of the iteration parameter. The iterations are terminated when the maximum magnitude of new velocity divergence becomes much less than the prescribed small value: $\max |D_{i,j}|^n<\epsilon$ (where, n is the iteration number and ϵ was usually taken to be 0.03). Physically, this condition means that the relative change of the fluid mass in each cell must not exceed 3% during the characteristic time L^2/ν_g. Note that $D^n_{i,j}$ may be easily found at each iteration as $D^n_{i,j}=-Eu\Delta t[\partial(\delta P)/\partial\tau]^n_{i,j}$. The final values of δP are used in Eq. (21) in order to compute the velocity field at time $(t+\Delta t)$.

The calculations are performed simultaneously both for the gas and liquid phases. The sequence of the steps inside each calculation cycle may be summarized as follows:

1) Calculate the new temperature (at $t+\Delta t$) in the internal points of both regions. Here, the explicit scheme with hybrid differencing of the convective terms[11] was applied to Eq. (4).

2) Calculate the new temperature along the walls and the liquid surface. Equations (13) and (14) are solved using the explicit scheme. The temperature on the gas/liquid interface is calculated from the finite-difference approximation of the boundary conditions in Eqs. (11) and (12).

3) Calculate the "tilde" velocities for the gas and liquid phases [Eq. (22)] and the interface velocities from the Eqs. (7) and (8).

4) Calculate the pressure change δP from the Poisson equation (25). For the typical computational run discussed below, usually two to six iterations are needed for the gas phase and two to four for the liquid phase.

5) Calculate the new velocity fields at $(t+\Delta t)$ and update the interface velocities. Go to step 1.

The calculations were performed with a 22×22 mesh in each phase. A denser mesh (32×32) was employed in one test case with no significant differences in the results. The time step was typically about 0.01 s and required about 1 s of CPU time on a VAX-11/750 computer. The computer code was tested by solving the standard problems of one-phase, steady-state cavity flows driven by shear[9] and buoyancy.[10] Our results are in good agreement with the literature when obtained with the same mesh sizes. For two-phase systems, no comparable data are presented in the literature (with the exception of the study[12] whose authors reported later an error in their computations).

Results and Discussion

The flowfield in the enclosure will be presented in terms of the streamlines. In the polar coordinate system, the nondimensional stream function $\psi(r,y)$ is related to the velocity components by

$$\psi=\int_0^r rv\,dr, \quad \psi=-r\int_0^y u\,dy \tag{26}$$

Test Case and Preliminary Remarks

Most calculations were made for the test case cylindrical enclosure ($R'=10$ cm, $H'=20$ cm) containing a water/air, two-layer system. The height of the liquid is 10 cm. The walls are given the properties for mild steel ($\rho_w=7800$ kg/m^3, $C_w=470$ J/kg·°C, $k_W=40$ w/m·°C); and wall thickness is taken to be $\delta_w=1$ mm. The radius of the hot source at the center of the top cover is $R_h'=2$ cm, and its temperature is maintained at $T_h'=1000$ K. The initial temperature in the enclosure was $T_0'=300$ K. Physical properties of the gas are calculated at the reference temperature $\bar{T}'=0.5(T_0'+T_h')$, while the liquid properties are taken at $T'=T_0'$. The Grashof number for the gas phase at normal gravity conditions is $Gr_g=3.05\times10^6$ and the Bond number is $Bo\simeq1400$.

The importance of radiative heat transfer for the problem in the present configuration is illustrated in Fig. 3, where the distributions of the radiant heat flux along the liquid and cylindrical surfaces are plotted at time $t=0$. The average radiant flux at the liquid surface is about 1100 W/m^2. To transfer the same flux from the gas by means of free convection with a typical heat-transfer coefficient of about 5 W/m°C, the temperature of the gas must be above 200°C. Thus, during the initial period, the liquid and side walls are heated primarily by thermal radiation.

Using the data from Fig. 3, we can calculate the temperature and velocity on the liquid surface at small times after the start of the process. During the initial short times $t'<t_\Delta'$, the thermal and velocity disturbances are transferred from the interface into the depth of liquid primarily by molecular diffusion. Convection plays no essential role. Using the classical solution for the transient one-dimensional heat conduction in a semi-infinite body with constant heat flux on the surface,[13] the local interface temperature may be written as

$$T_{lg}'=T_0'-Aq_R'\sqrt{t'} \tag{27}$$

where

$$A=2/[\pi^{1/2}(\sqrt{\rho_\ell C_{p_\ell}k_\ell}+\sqrt{\rho_g C_{p_g}k_g})]$$

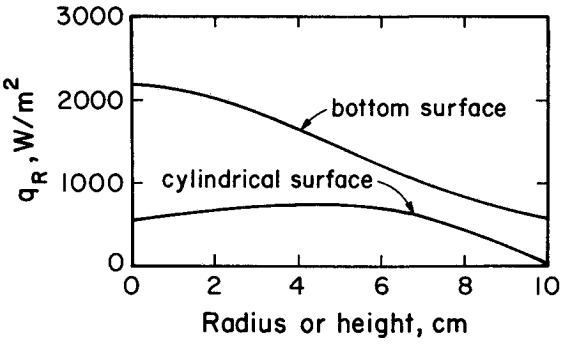

Fig. 3 Radiative heat flux on the liquid surface and the side wall at time $t'=0$.

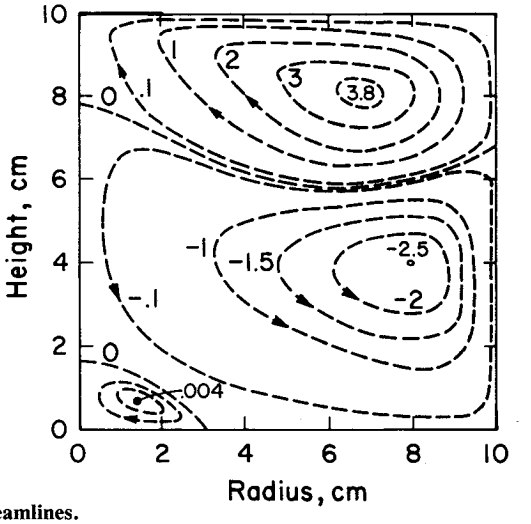

a) Streamlines.

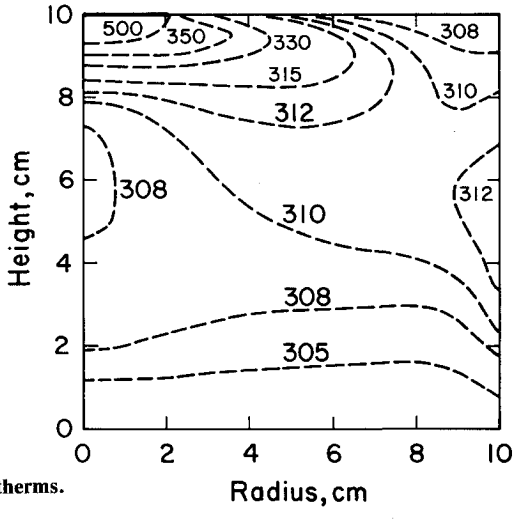

b) Isotherms.

Fig. 4 Contours in the gas phase for the one-fluid problem at $t'=100$ s ($Gr_g=3.05\times10^6$).

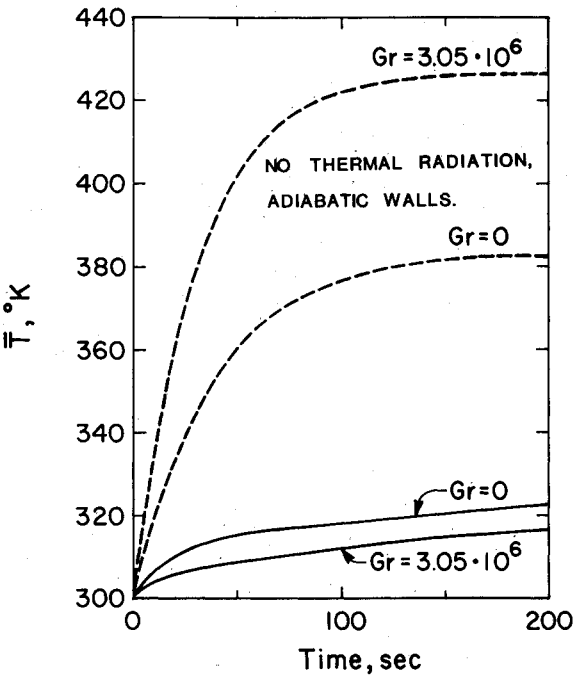

Fig. 5 Volume-averaged gas temperature as a function of time in one-fluid problem (dotted lines: simplified model without thermal radiation, adiabatic walls).

The velocity gradient induced by the variation of the surface tension is now expressed from Eq. (7) in the form

$$\left(\frac{\partial u'}{\partial y'}\right) \simeq \frac{\sigma_T}{\mu_\ell} A \left(\frac{d\bar{q}'_R}{dr'}\right) \sqrt{t'} \tag{28}$$

where $\sigma_T = d\sigma/dT'$ and the viscous stresses in the gas near the interface are assumed to be very small in comparison with those in the liquid. The velocity disturbance propagates into the liquid according to the equation for the transient diffusion of momentum,

$$\frac{\partial u'}{\partial t'} = \nu_\ell \frac{\partial^2 u'}{\partial y'^2} \tag{29}$$

The solution of this equation, subject to the boundary conditions [Eq. (28)] and $u' = 0$ at $y \to \infty$ may be also found in Ref. 13. For the surface velocity, one finally obtains

$$u'_{\ell g} \simeq \frac{\sigma_T}{2\rho_\ell k_\ell \sqrt{Pr_\ell}} \left(\frac{dq'_R}{dr'}\right) t' \tag{30}$$

In the test case shown in Fig. 3, $dq'_R/dr' \simeq 16 \times 10^3$ W/m^3 and the average surface velocity increases approximately as $\bar{u}_{\ell g} = 10^{-3} t$ m/s. The Reynolds number based on this velocity, cavity radius, and liquid viscosity is $\overline{Re}_\sigma = 1200$ after $t' = 10$ s. It is apparent now that the subsurface liquid flow should be a boundary-layer type. The average thickness of this boundary layer is $\delta \simeq 3R'/\sqrt{Re_\sigma}$ and the time t'_Δ may be estimated as $t'_\Delta \simeq \delta^2/\nu_\ell$. For the test case conditions, $t'_\Delta \simeq 30$ s.

Estimates show that the thermal inertia of the walls is also a very important factor in the thermal regime at the upper part of the enclosure. The average radiative flux on the side wall is about $\bar{q}'_R \simeq 500$ W/m^2. Part of this heat is accumulated by the wall, while the remainder is transferred to the gas. The increase in the wall temperature, $\Delta T'_w = T'_w - T'_0$, during the short time interval $\Delta t'$ may be estimated by assuming that the heat transfer from the wall to the gas occurs primarily by transient conduction. Then, from Ref. 13, $\Delta T'_w \sim (2\bar{q}'_{wg}/k_g)\sqrt{\alpha_g \Delta t'/\pi}$, where $\bar{q}'_{wg}$ is the time-averaged heat flux transferred from the wall to the gas phase.

If the thickness of the wall is infinitesimally small ($\delta_w \to 0$), then $\bar{q}'_{wg} = \bar{q}'_R$, which yields $\Delta T'_w \simeq 106$°C at $\Delta t' = 1$ s. This large value is, of course, a physically meaningless result. In reality, with a wall thickness of $\delta_w = 1$ mm, the maximum temperature growth does not exceed the value $\Delta T'_w < \bar{q}'_R \Delta t'/(\rho_w C_w \delta_w) \sim 0.14$°C. Note that the total heat capacity of the walls at the upper part of the enclosure is approximately 200 times greater than the total heat capacity of the gas phase. Clearly, the heating rate of the gas in the container is controlled by the thermal inertia of the walls and liquid.

It is interesting that the same conclusion remains valid even if the walls are made from a poorly conductive material. In this case, the wall surface temperature will not exceed the value $\Delta T'_w \doteq 2\bar{q}'_R \sqrt{\Delta t'/(\pi k_W \rho_W C_W)}$. For intance, for the common brick wall ($\rho_W = 1900$ kg/m^3, $C_W = 800$ J/kg·K, $k_w = 0.7$ W/m·K) $\Delta T'_W$ is less than 5.5°C after $\Delta t' = 100$ s.

Decoupled Gas-Phase Calculations

We consider first the simple case of heat transfer and fluid motion in the gas phase only, assuming that the liquid surface is motionless and maintained at the constant temperature $T' = T_0$.

Figures 4a and 4b present streamline and isotherm contours at $t' = 100$ s and normal gravity conditions. Positive and negative values of ψ correspond to clockwise and counterclockwise circulation, respectively. Near the hot source, gas moves along the top cover in the outward radial direction. At $t' = 100$ s, the flowfield consists of two large vortices whose intensities are of the same order of magnitude and a weak third vortex at the center of the bottom. Note that the free convective motion of the gas arises first in the vicinity of the hot spot and, initially, a single positive circulating vortex ring occupies the full volume of the gas cavity. At $t' \sim 1$ s, the small secondary negative vortex originates at the corner of the bottom. As time elapses and the side wall is heated by thermal radiation, the free-convective currents near this wall strengthen the secondary vortex and slightly weaken the circulation in the primary vortex.

One of the interesting characteristics of the fluid motion inside a particular vortex ring is the average period of circulation, which can be estimated as

$$\bar{t}_{\text{circ}} = \frac{t'_{\text{circ}}}{t'_*} = \frac{W}{2\pi(\psi_{\max} - \psi_{\min})} \tag{31}$$

where W is the volume of the circulating vortex and $\psi_{\max}$, $\psi_{\min}$ the maximum and minimum values of the stream function inside the vortex. Using Eq. (31), we find that the circulation periods for the vortices shown in Fig. 4a are equal to about 8 and 22 s for the primary and secondary vortex, respectively. For the third vortex at the center of the bottom, $\bar{t}_{\text{circ}} \sim 100$ s.

The isotherms in Fig. 4b indicate that substantial increase in the temperature occurs only in the small region near the hot source. In Fig. 5, the volume-averaged temperature of the gas is plotted as a function of time for different cases. We consider first the cases shown by dotted lines, for which the thermal radiation was neglected and the walls assumed to be adiabatic ($\partial T/\partial n = 0$). Such a model is considered in more detail in Refs. 4 and 14. It predicts the "normal" behavior of the gas heating rate, which increases with the growth of the Grashof number. At time $t' = 200$ s, the average temperature of the gas approaches its asymptotic value and the steady-state thermal regime is established in the gas phase.

The solid curves in Fig. 5 refer to the more realistic model of the transport processes, including both the effects of thermal radiation and wall thermal inertia and conductance. Surprisingly, the heating rate of the gas appears to be considerably slower than before. In addition, the volume-averaged gas temperature in the zero-gravity case ($Gr = 0$) is found to be lower than that at normal gravity conditions ($Gr = 3.05 \times 10^6$). To explain this phenomenon, it may be noted that a major part of the heat obtained by the gas from the hot source is

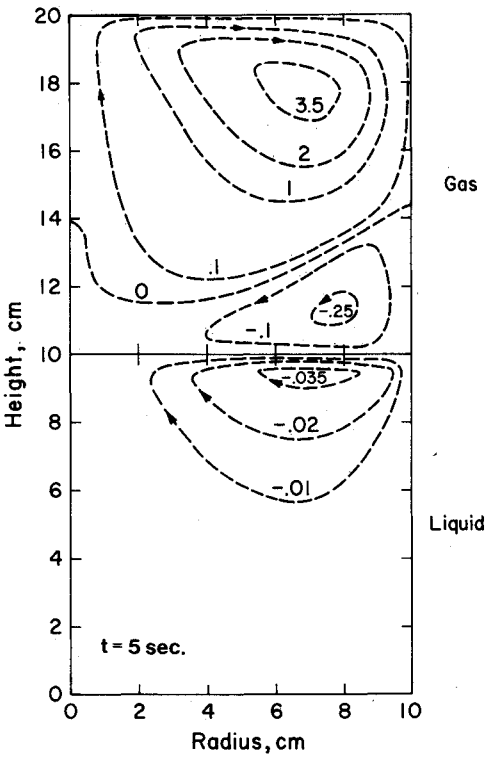

a) Streamlines, $t' = 5$ s.

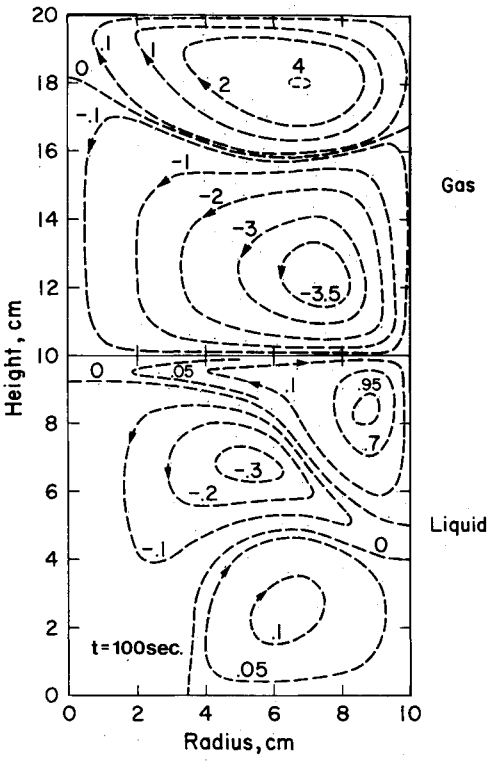

c) Streamlines, $t' = 100$ s.

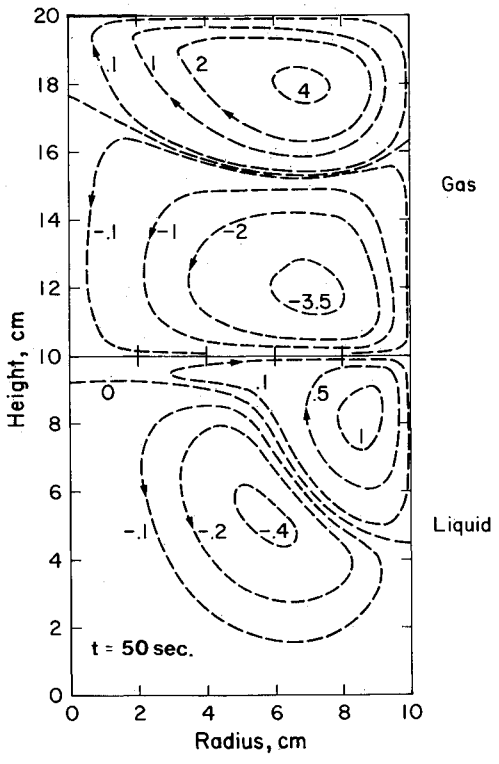

b) Streamlines, $t = 50$ s.

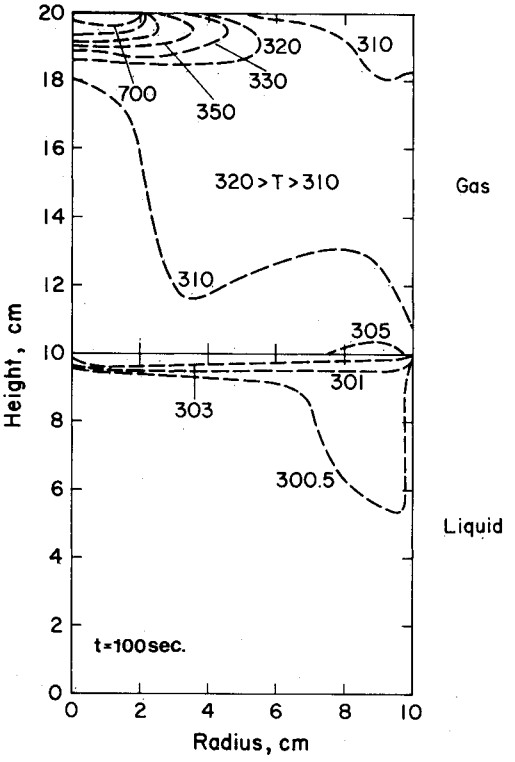

d) Isotherms, $t' = 100$ s.

Fig. 6 Streamline and isotherm contours at normal gravity ($Gr_g = 3.05 \times 10^6$) and different times.

transferred via convection to the cold top wall. This strong convective cooling is not present in the zero Grashof number case. Note also that the surface area of the cold top wall is 24 times greater than the area of the hot spot. In the presence of gas motion, the heat transfer from the hot spot increases. But simultaneously, the convection causes better spreading of the hot gas along the top cover and, accordingly, the heat lost by the gas increases.

Various components of the heat flow balance in the enclosure are presented in Table 1 at time $t' = 20$ and 200 s.

From Fig. 5 it is evident that the steady-state thermal regime is far from being attained at $t' = 200$ s. This lag occurs because the wall temperature increases very slowly and the temperature distribution in the gas must adapt itself to the continuously changing boundary conditions. Also, note that the average period of gas circulation in the enclosure is about 15 s.

Two-Fluid System

Now we examine the two-fluid system, taking into consideration that the transport processes in both phases are coupled on the interface through the boundary conditions established in Eqs. (7), (8), (11), and (12).

It must be noted that the finite-difference approximation for the interface temperature yields a considerable truncation error at small times. For example, at the first time step, the interface temperature $T_{\ell g}$ is calculated from

$$q'_R = k_\ell \left(\frac{T_{\ell g} - T_0}{0.5 \Delta y'_\ell} \right) + k_g \left(\frac{T_{\ell g} - T_0}{0.5 \Delta y'_g} \right) \tag{32}$$

where Δy_ℓ and $\Delta y'_g$ are the mesh sizes in vertical direction for the liquid and gas phases, respectively.

For the test case geometry with $\Delta y'_\ell = \Delta y'_g = 0.5$ cm and $q'_R \simeq 2000$ W/m^2, one obtains $T'_{\ell g} \simeq 307.6$ K. This value seems to be too large; in addition, it does not depend on the time step. The error results from the assumption implied in Eq. (32) that the thermal disturbance immediately penetrates the distance $0.5\Delta y_\ell$ into the liquid. In truth, however, the time required for the disturbance to propagate this distance is of order $0.25\ \Delta y'^2_\ell / \alpha_\ell$, which is about 40 s in our case and considerably greater than the time step $\Delta t' \simeq 0.01$ s. To overcome this difficulty, we can assume that, during an initial short time $t' \ll t'_\Delta$, the surface temperature and velocity may be calculated from the analytical solutions of Eqs. (27), and (30).

Note that the finite-difference solution also would predict the time-independent local value of the surface velocity at short times,

$$u_{\ell g} = \frac{\sigma_T \Delta y'^2_\ell}{4 \mu_\ell K_\ell} \left(\frac{dq'(r)}{dr'} \right) \tag{33}$$

In the present study, the analytical solutions (27) and (30) were used at times less than $t' = 0.5\ \Delta y'^2_\ell\ \sqrt{Pr_\ell / \nu_\ell}$. At this time, the analytical and finite-difference values of $u_{\ell g}$ are equal.

We start the discussion of the numerical results with Figs. 6a–6c, where the temporal development of the velocity field at normal gravity is illustrated at times $t' = 5$, 50, and 100 s, respectively. The isotherms at $t' = 100$ s are shown in Fig. 6d. Note that both thermal radiation and transient heat conduction in the walls are taken into account. The nonuniform radiant flux on the liquid (Fig. 3) results in a temperature gradient along the liquid surface. In turn, this gradient induces surface-tension-driven convection in the gas and liquid phases at both sides of the interface. The patterns of the gas motion are very similar to those obtained in the one-fluid case (Fig. 4a). However, the circulation in the negative vortex at large times is now strengthened due to a contribution made by the surface forces.

The liquid motion is initially a weak single vortex whose intensity increases monotonically with time. At larger times, this vortex is separated into two and later into three vortices. From inspection of the isotherm contours in Fig. 6d, it is inferred that the buoyancy forces are responsible for the disintegration of the primary vortex. Such a vortex disintegration is not observed under reduced gravity conditions and lower Grashof number (see Fig. 7a).

Figure 7 shows the flow and temperature fields occurring at low gravity, $g = 10^{-4}$ m/s^2 ($Gr_g \simeq 31.2$). Surface tension induces a single vortex in each phase, while buoyancy convection does not play any role. Near the axis of symmetry, the gas moves toward the bottom and, hence, the isotherms under the hot source are elongated in the same direction. Since the hot gas does not spread along the cold top wall, the heat loss transferred from the gas to the walls is smaller and the average gas temperature higher than in the case of normal gravity. This conclusion is also supported by Fig. 8 where the average gas temperatures are plotted vs time at normal and reduced gravities. In the same figure, the maximum and minimum temperatures on the gas/liquid interface are presented. Note that the maximum and minimum of the liquid-surface temperature are always observed at the center and in the vicinity of the side wall, respectively.

Figure 9 exhibits the temperature and velocity distributions along the gas/liquid interface at $t' = 100$ s. In the case of reduced gravity, the surface temperature gradients and velocities are slightly higher than those at normal gravity. The fact that surface values for the two differ only slightly indicates that radiation and surface tension are the most important factors governing the temperature and velocity distributions along the gas/liquid interface.

In Fig. 10, the horizontal velocity profiles $U = U(y)$ at mid-radius $r = 0.5$ are given for both liquid and gas phases at $t' = 100$ s. These data, together with Figs. 6d and 7b, show that the major changes of liquid velocity and temperature occur in a thin region very close to the surface. After the initial transient period of about 50 s duration, the temperature and velocity on the liquid surface vary very slowly (see Fig. 8). This quasi-steady behavior may be an indication that both the thermal and dynamic boundary layers have already stabilized.

The average temperature on the liquid surface is $T_{g\ell} = 306$ K. Note that the liquid in the container is heated primarily by thermal radiation. The time required for the entire liquid to approach the average temperature $T_{g\ell}$ is estimated to be 2400 s. Therefore, for the present configuration, the characteristic times of stabilization of the thermal and velocity boundary layers below the surface are much shorter than the characteristic time of heating of the liquid in the container. After the initial transient, the hydrodynamic and thermal processes in the liquid boundary layer at the interface may be considered as quasi-steady.

The Grashof number for the liquid phase has been previously determined in Eq. (3) using the reference temperature

Table 1 Components of heat flow at $t' = 20$ and 200 s, W

	Grashof No.			
	0		3.05×10^6	
	Time, s			
Component of heat flow	20	200	20	200
Convective transfer				
From hot spot	4.17	4.09	7.91	7.61
To the liquid surface	0.35	0.95	0.15	0.89
To the top wall (excluding hot spot)	3.55	3.64	7.82	7.59
From the side wall	0.55	0.57	0.24	0.96
Heating of the gas	0.32	0.07	0.18	0.09
Radiative flow				
To the liquid	35.1	37.9	35.5	38.4
To the side wall	35.4	33.1	35.2	33.6
Average temperature of the gas, K	312.3	322.7	304.5	316.8

Table 2 Parametric study of the gravitation, radiation, and surface tension effects

Run no.	g/g_n	Rad[a]	Surface tension[a]	$V_{g,\max}$, cm/s	$U_{\ell g,\max}$, cm/s	$T_{\ell g,\max}$, K	Re_ℓ^p	Gr_ℓ^p	Ma_ℓ^p
1	1	1	1	4.97	4.97	309.77	6010.	2.4×10^7	8.5×10^5
2	1	1	0	4.03	0.96×10^{-2}	313.02	11.6	2.9×10^7	0
3	1	0	1	4.18	0.83×10^{-2}	300.003	10.04	1.2×10^4	420
4	1	0	0	4.18	0.75×10^{-2}	300.003	9.07	1.2×10^4	0
5	10^{-2}	1	1	5.21	5.21	309.42	6300.	2.46×10^5	8.8×10^5
6	10^{-2}	1	0	0.79	0.69×10^{-2}	315.63	8.4	$4.\times10^5$	0
7	10^{-2}	1	0	0.80	0.6×10^{-1}	300.033	72.	1.2×10^3	$1.\times10^6$
8	10^{-2}	0	0	0.80	-0.3×10^{-2}	300.033	3.63	1.2×10^3	0
9	10^{-4}	1	1	5.51	5.51	310.31	6670.	2.8×10^3	$1.\times10^6$
10	10^{-4}	1	0	0.25×10^{-1}	0.6×10^{-4}	315.78	7.3×10^{-2}	4×10^3	0
11	10^{-4}	0	1	0.217	0.217	300.168	260.	58.4	2.1×10^4
12	10^{-4}	0	0	0.026	-0.145×10^{-3}	300.184	1.75	71.1	0

[a]The value 1 or 0 in these columns means that the radiation (surface tension) effect is present or absent, respectively.

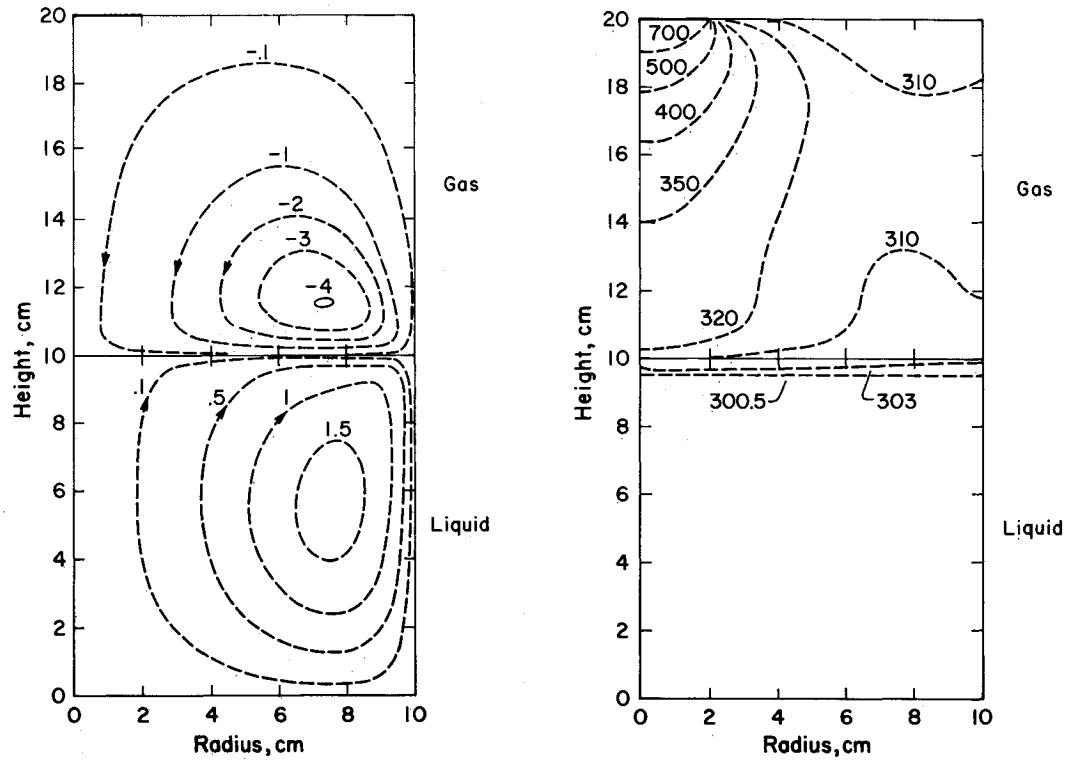

a) Streamlines. b) Isotherms.

Fig. 7 Contours at $t'=100$ s (reduced gravity, $g=10^{-4}$ m/s^2, $Gr_g=31.1$).

difference $\Delta T'_* = T'_h - T'_0$ (=700°C). However, the actual temperature drop in the liquid is much lower and does not exceed the value $\Delta T' = T'_{\ell g,\max} - T'_0$. Here, $T'_{\ell g,\max}$ is the maximum surface temperature. Therefore, the actual Grashof number governing the natural convection in the liquid volume may be expressed as

$$Gr_{\ell,p} = g\beta_\ell R'^3 (T'_{\ell g,\max} - T'_0)/\nu_\ell^2 \tag{34}$$

where subscript p denotes that this parameter is not known beforehand and needs to be determined experimentally or by a numerical analysis a posteriori.

The other fundamental dimensionless parameter of the problem is the Marangoni number

$$Ma_{\ell,p} = \sigma_T \Delta T'_{\ell g} R'/(\mu_\ell \alpha_\ell) \tag{35}$$

which is also evaluated a posteriori. Here $\Delta T'_{\ell g}$ is the temperature drop along the liquid surface. The Marangoni number governs the intensity of the convection in the thermocapillary flows.[15] In particular, for the boundary-layer flows induced by the surface-tension gradient, the surface velocity may be estimated from the expression

$$\overline{Re}_\sigma = \bar{U}'_\sigma R'/\nu_\ell \sim (Ma/Pr_\ell)^{2/3} \tag{36}$$

In the general case, however, the pre-estimation of the surface velocity is a difficult task, especially for the present configuration with the heating from above. To classify the structure of the subsurface flow, we introduce the Reynolds number

$$Re_{\ell,p} = U_{\ell,\max} R'/\nu_\ell \tag{37}$$

Table 2 illustrates some results of the parametric study of how gravity, radiation, and surface tension affect the surface velocity and temperature. These results refer to the standard geometry case and the time $t'=100$ s. The value $v_{g,\max}$ denotes

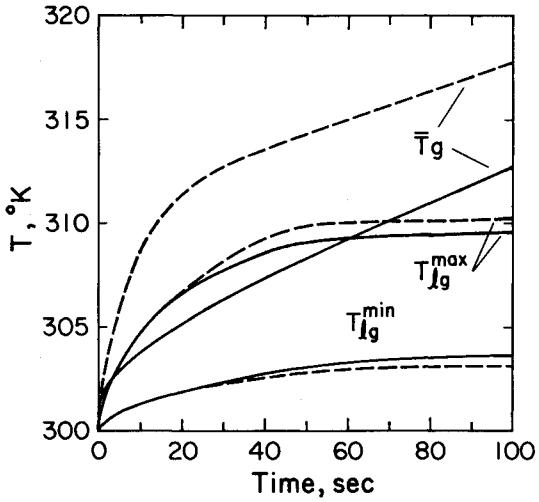

Fig. 8 Volume-averaged gas temperature and the maximum and minimum liquid surface temperature as functions of time (standard case, air/water system, ____ $g/g_n = 1$, --- $g/g_n = 10^{-4}$).

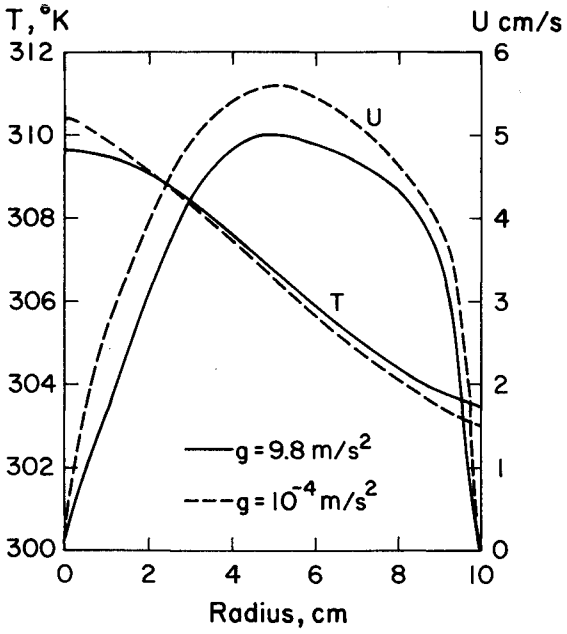

Fig. 9 Temperature and velocity along the gas/liquid interface ($t' = 100$ s).

the maximum velocity in the gas phase. A few conclusions can be drawn from Table 2 as follows:

1) When both radiation and surface tension effects are taken into the consideration (runs 1, 5, 9), the surface velocity is at least one order of magnitude greater than in all other cases. The maximum fluid velocity in the system occurs on the gas/liquid interface. The subsurface flow is a boundary-layer type.

2) When the surface tension effect is not included (runs 2, 6, 10), the surface velocity is considerably lower. The surface temperature, however, is larger than that in the previous case due to the weaker mixing.

3) When radiation is neglected but the surface tension effect is included (runs 3,8,11), the surface velocity increases with the reduction of the gravity.

4) When both radiation and surface tension are not considered, the surface velocity is negligibly small.

It is interesting to note that at low gravity conditions, the surface velocity induced by the surface-tension gradients may

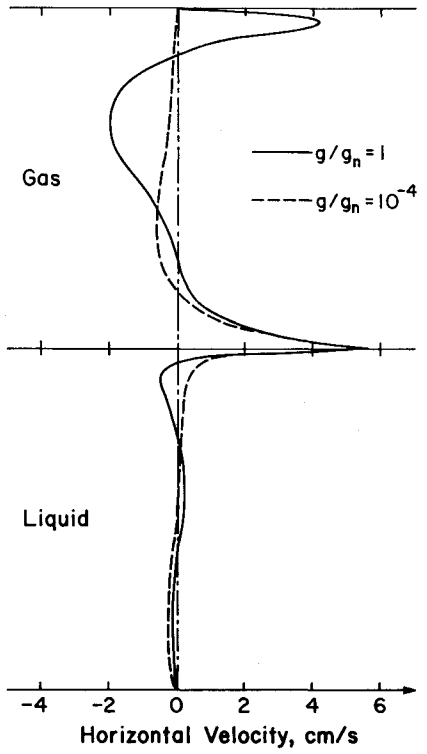

Fig. 10 Horizontal velocity profiles at mid-radius (standard geometry, air/water system, $t' = 100$ s).

be reasonably estimated using Eq. (33) (see runs 9, 11). All of the above results were obtained for the water/air system. In addition, the calculations have been made for the case of the *n*-decane-air system with the standard geometry and normal gravity conditions. The flow pattern in the gas phase is qualitatively similar to that of the water/air case; however, more circulatory cells occur in the liquid phase. Both the temperature and velocity on the surface of the decane are considerably higher than in the case of water. To explain these results, it may be noted that the thermal conductivity of the liquid decane is approximately five times less than the conductivity of water. Thus, the thermal resistance of the surface layer is considerably higher.

Conclusions

The time-dependent fluid flows and thermal transport associated with the nonuniform heating from above of a two-layer gas-and-liquid enclosure have been investigated by finite-difference methods. The calculations demonstrated the great importance of including the effects of thermal radiation and thermal inertia of the walls bounding the enclosure. Nonuniform radiative heating of a liquid surface appears to be the principal factor in the initiation of a surface-tension-driven convection along the gas/liquid interface. The thermal inertia of the walls controls the temperature growth in the gas phase. The gas and liquid motions are the net result of both surface tension and buoyancy forces.

Future study of this problem should include the effects of variable density of the gas phase, liquid evaporation, diffusion, and chemical reaction for specific air-fuel systems. Allowances for nonblack walls and gas radiation transfer are also of interest. In order to improve the accuracy of the numerical simulation in the subsurface layer, a nonuniform refined grid should be used in this region.

References

[1]Murad, R. J., Lamendola, J., Isoda, M., and Summerfield, M., "A Study of Some Factors Influencing the Ignition of a Liquid Fuel Pool," *Combustion and Flame*, Vol. 15, 1970, pp. 289-298.

[2]Sirignano, W. A. and Glassman, I., "Flame Spreading Above Liquid Fuels: Surface-Tension-Driven Flows," *Combustion Science and Technology*, Vol. 1, 1970, pp. 307.

[3]Furita, M., Humphrey, J. A., and Fernandez-Pello, A. C., "Prediction of Flame Spread Hydrodynamics Over Liquid Fuel," *Physico Chemical Hydrodynamics*, Vol. 6, No. 4, 1985, pp. 347–372.

[4]Aggarwal, S. K., Iyengar, J., and Sirignano, W. A., "Enclosed Gas and Liquid with Nonuniform Heating from Above," *International Journal of Heat and Mass Transfer*, to be published.

[5]Siegel, R. and Howel, J. R., *Thermal Radiation Heat Transfer*, 2nd ed., Hemisphere, New York, 1984.

[6]Amsden, A. A. and Harlow, F. H., "The SMAC Method," Los Alamos Scientific Laboratory, Los Alamos, NM, Rept. LA-4370, 1970.

[7]Hirt, C. W., Nichols, B. D., and Romero, N. C., "SOLA-A Numerical Solution Algorithm for Transient Fluid Flows," Los Alamos Scientific Laboratory, Los Alamos NM, Rept. 5852, 1975.

[8]Mitchell, A. R. and Griffiths, D. F., *The Finite-Difference Method in Partial Differential Equations*, Wiley, New York, 1980.

[9]Torrance, K. et al., "Cavity Flows Driven by Buoyancy and Shear," *Journal of Fluid Mechanics*, Vol. 51, Pt. 2, 1982, pp. 221–231.

[10]De Vahl Davis, G. and Jones, I. P., "Natural Convection in a Square Cavity, A Comparison Exercise," *Numerical Methods in Thermal Problems*, edited by R. W. Lewis et al., Pineridge Press, Swansea, Wales, 1981, pp. 553–572.

[11]Patankar, S. V. *Numerical Heat Transfer and Fluid Flow*, Hemisphere/McGraw-Hill, New York, 1980.

[12]Knight, R. W. and Palmer, M. E. III, "Simulation of Free Convection in Multiple Fluid Layers in an Enclosure by Finite-Differences," *Numerical Properties and Methodologies in Heat Transfer*, edited by T. M. Shih, Hemisphere, New York, 1983, pp. 305–319.

[13]Carslaw, H. S. and Jaeger, J. C., *Conduction of Heat in Solids*, 2nd ed., Oxford University Press, New York, 1959.

[14]Abramzon, B., Edwards, D. K., and Sirignano, W. A., "Transient Natural and Surface-Tension-Driven Convection in a Two-Layer Gas-and-Liquid Enclosure with Nonuniform Radiative Transfer," AIAA Paper 86–0578, 1986.

[15]Ostrach, S., "Low-Gravity Fluid Flows," *Annual Review of Fluid Mechanics*, Vol. 14, 1982, pp. 313–345.